Open Access

PANDA Type Four-Core Fiber With the Efficient Use of Stress Rods

Yi Yang
Jitao Gao
Songnian Fu
Xinben Zhang
Ming Tang
Weijun Tong
Deming Liu
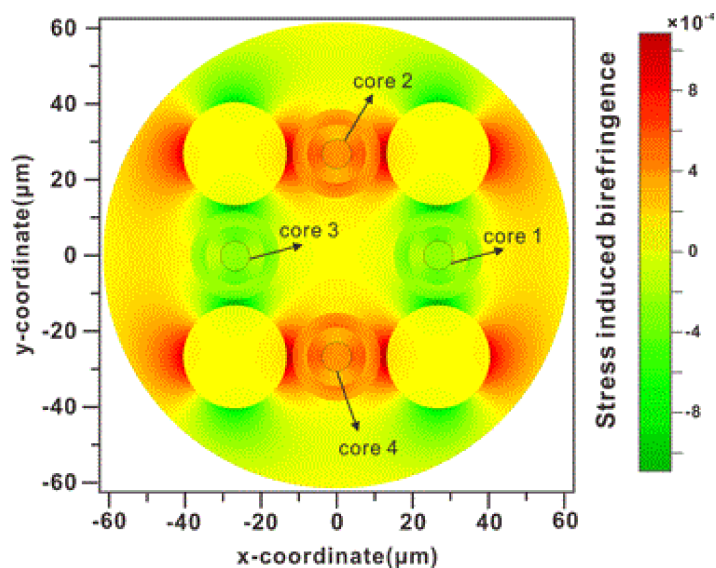
photonics SOCIETY

IEEE

PANDA Type Four-Core Fiber With the Efficient Use of Stress Rods

Yi Yang,[1] **Jitao Gao** ⓘ **,**[1] **Songnian Fu** ⓘ **,**[1] **Xinben Zhang** ⓘ **,**[2]
Ming Tang,[1] **Weijun Tong,**[2] **and Deming Liu**[1]

[1]Wuhan National Laboratory for Optoelectronics, School of Optical and Electronic Information, Huazhong University of Science and Technology, Wuhan 430074, China
[2]State Key Laboratory of Optical Fiber and Cable Manufacture Technology, Yangtze Optical Fiber and Cable Joint Stock Limited Company, Wuhan 430074, China

Abstract: We design a panda type four-core fiber with a comparable optical property of the polarization maintenance single mode fiber (PM-SMF) and can support 8 non-polarization-degenerate eigenmodes with a birefringence of approximate 3.24×10^{-4} over the wavelength range from 1288 to 1630 nm. In particular, only four stress rods are efficiently used to achieve the PM characteristics for each core, in comparison with traditional design of panda type PM-SMF. Meanwhile, we identify that the optimal configuration of stress rods can not only enhance the birefringence, but also further suppress the crosstalk (XT) between two primary eigenstate of polarization (ESOP) arising in adjacent cores, although the corresponding XT at secondary ESOP remains unchanged. Moreover, our numerical results show that both chromatic dispersion (CD) together with mode field diameter (MFD) and the bending sensitivity are consistent among four cores. We believe that such specialty multi-core fiber is ideal for compact and cost-effective fiber-optic gyroscope (FOG) application, besides the potential in the MIMO-free spatial division multiplexing (SDM) interconnection.

Index Terms: Polarization maintaining fiber, multicore fiber, fiber-optic gyroscope.

1. Introduction

The soaring requirement of datacenter (DC) interconnects may lead to the quick occurrence of capacity crunch of standard single mode fiber (SSMF) in the future. Space division multiplexing (SDM) is the alternative technique to cope with such problem [1]–[3]. As for the SDM technique, spatially separated channels can be used to transmit multiple-channel signals simultaneously. Few-mode fiber (FMF) has demonstrated its potentials for fulfilling such motivation [4], [5]. However, there are some disadvantages associated with the FMF with a large number of spatial modes, although it is not challenging to increase the number of spatial modes arising in the FMF. First, the confinement factor and consequently the bending loss of the high-order modes are degraded severely than that of low-order modes [6]. Secondly, (de)multiplexing among a large number of modes is complex and generally introduces more insertion losses [7]. Since multicore fibers (MCFs) can provide parallel spatial channels to improve the transmission capacity, there exist abundant researches by using the MCF for the DC interconnection [8]–[10]. In order to expand the transmission capacity of MCF,

an effective way is to increase core numbers [11] or the mode numbers arising in corresponding core of MCF [12]. Although the common method to suppress the crosstalk (XT) between the adjacent cores is to enlarge the cladding diameter, it is undesired in terms of fiber reliability and high-density core arrangement. By considering the SDM fibers as a viable solution of DC photonic interconnects, it is ideally to (a) increase the number of spatial channels within the constraints of 125 μm diameter cladding, and (b) allow the independent detection of the spatial channel without the multiple-input and multiple-output (MIMO) processing. Recently, 8-core fiber with a cladding size of 125 μm has been demonstrated for the O-band transmission [13]. However, the scalable design of spatial channel for the MCF is annoyed, due to the reduction of either core-to-core or core-to-coating distances, because the former will foster the inter-core XT and the later will bring about external leakage loss of the cores. Generally, for the application of DC interconnects, 4-core fiber with a cladding size of 125 μm, which features comparable optical property with SSMF, has the competitive upgrading capability from the existing SSMF infrastructure by a step by step manner [14]. Meanwhile, the fiber-optic gyroscope (FOG) by relying on the non-reciprocal Sagnac effect, has been verified its excellent performance in interial guidance systems [15]. Generally, the interferometer FOG (I-FOG) employs typical 1 km polarization maintaining SMF(PM-SMF) coil to enhance the sensitivity [16], leading to a large package and heavy weight. When multiple PM channels without the XT can be provided, the consumption of PM-SMF can be saved, so as to make the I-FOG light and compact. Besides, double ring structure is commonly used to improve the detection sensitivity of the resonator FOGs (R-FOGs) [17], but it is challenging to control the length mismatch under the scale of sub-wavelength between two fibers [18]. In case double rings are realized by the MCF, the length mismatch is convenient to manage so as to notably reduce the fabrication difficulty. Furthermore, in order to avoid the thermal effect induced instabilities, two eigenstate of polarizations (ESOPs) of the PM-SMF are simultaneously excited [19]. However, for the ease of two-ESOP orthogonal propagation, the configuration of traditional PM-SMF coil is complicated and susceptible to the imperfect splice [20], [21].

In this paper, we propose a panda type 4-core single-mode fiber with a cladding size of 125 μm, whose mode field diameter (MFD), dispersion, and beat length, are comparable to a traditional PM-SMF. Such fiber can double the interconnection capacity without the use of MIMO technique, in comparison with the traditional 4-core fiber. Because of the stress rods induced birefringence, the polarization mixing between the ESOPs for each core is successfully mitigated. Consequently, 8 spatial channels with a birefringence (δNeff) of approximate 3.24×10^{-4} can be obtained over O+C+L bands (1288-1630 nm). In particular, we only use four stress rods to achieve the PM characteristic for each core. In comparison with the traditional panda-type PM-SMF, both the efficient use of stress rods and the cost reduction are realized with the successful mitigation of the inter-core XT.

2. Fiber Structure and Design Strategy

The transverse section and the relative refractive index (RI) distribution of the panda type 4-core fiber is schematically shown in Fig. 1(a) and (b), respectively. The parameter r is the radius of four stress rods. 2d is the distance between the center of the stress rods. The core pitch Λ is equal to $\sqrt{2}$d. We can see that the stress rods are placed at the corner of the square that has a length of 2d, and the cores are located at the center of each side. Such arrangement, for the purpose of the photo-elastic induced birefringence of individual cores, is sufficiently generated by the adjacent stress rods. Meanwhile, we set the core diameter 2ρ of 8 μm and relative RI difference $\triangle_1$ between the core and the cladding of 0.35%, in order to maintain almost the same optical properties as the SSMF. Since small inter-core XT is compulsory for the MCF transmission, we use the trench configuration for the ease of XT reduction. Here, a and w are the inner radius and width of the trench, respectively. Generally, the inner radius of the trench a/ρ is more than 2.0, in order to avoid the reduction of the MFD, we set a = 2ρ and the trench width w = ρ, respectively. Initially, r is set as 0 μm so that the birefringence is not taken into account. Since the inter-core XT is proportional to the operation wavelength [22], we start to investigate the inter-core XT between adjacent cores
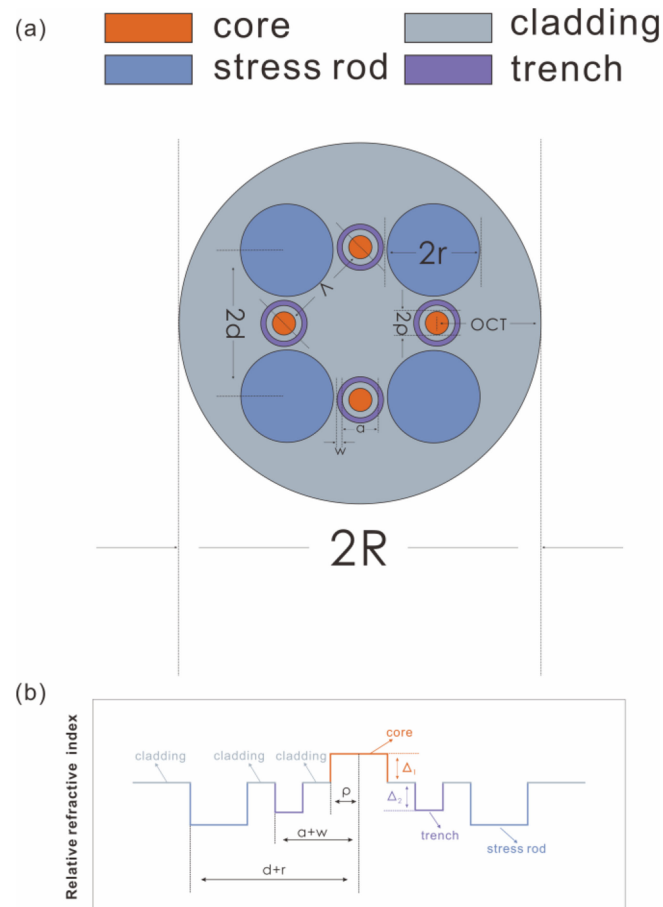
Fig. 1. (a) Transverse section of the dual panda type 4-core-MCF and the corresponding (b) relative refractive index distribution.

at 1630 nm as the function of the relative RI difference, trench Δ_2, and core pitch Λ. We use the coupled power theory (CPT) and finite element method (FEM), as shown in Eq. (1)

$$XT = 2\frac{\kappa^2 \cdot R}{\beta \cdot \Lambda} \cdot L \qquad (1)$$

where β, R, and L are the propagation constant, bending radius, and fiber length, respectively. In this work, we set L = 100 km and R = 140 mm to consider a target inter-core XT of -40 dB over the O+C+L bands. The coupling coefficient $\kappa = \kappa_{ij} = \kappa_{ji}$ between core i and j can be described by Eq. (2) [23]

$$\kappa = \frac{\omega\varepsilon_0 \iint (N - N_j^2)E_i^* \cdot E_j ds}{\iint u_z \times (E_i^* \times H_i + E_i \times H_i^*)ds} \qquad (2)$$

where ω is angular frequency, ε_0 is the vacuum permittivity, and u_z means the outward-directed unit vector. N denotes the RI distribution of the fiber and N_j represents that of the core j. The E_i and E_j denote the electric field distribution of the core i and the core j, respectively. H_i represent the magnetic field distribution of the core i. The result is shown in Fig. 2. Obviously, larger Λ and Δ_2 are more likely to reduce the XT between adjacent cores, where Λ and Δ_2 range from 35 to 45 μm and -0.42% to -1.39%, respectively. Meanwhile, the outer cladding thickness (OCT) is another important factor that need to be considered, which is the distance between the fiber edge
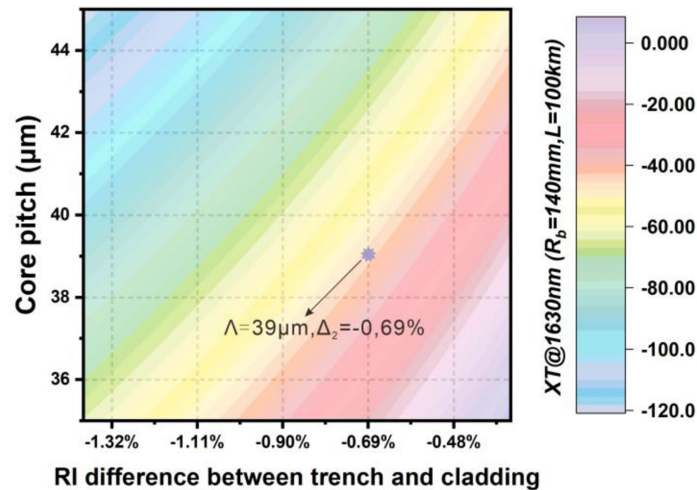
Fig. 2. Crosstalk between adjacent cores as the function of the RI difference between trench and cladding, and the core pitch Λ.

TABLE 1

Mechanic Parameters of the Fiber

	Quality	Core	Cladding	Stress Rods	Trench
α	Thermal expansion coefficient(K^{-1})	7.9×10^{-7}	5.4×10^{-7}	1.96×10^{-6}	1.01×10^{-6}
E	Young's modulus (Pa)	7.05×10^{10}	7.25×10^{10}	5.28×10^{10}	6.51×10^{10}
v	Poisson's ratio	0.183	0.186	0.219	0.149
ρ	Density(kg·m^{-3})	2267	2196	2169	2187
B_1	First stress optical coefficient (Pa^{-1})	6.5×10^{-13}			
B_2	Second stress optical coefficient (Pa^{-1})	4.2×10^{-12}			
T_0	Drawing temperature(°C)	2200			
T_1	Operating temperature(°C)	20			

and the center of the core. i.e., OCT = R-d. It is identified that both larger OCT and larger Δ_2 are helpful to avoid the micro bending loss and excess leakage loss of cores [24]. By considering of those parameters mentioned above, we set $\Lambda = 39\ \mu m$ and $\Delta_2 = -0.69\%$, respectively. The cut-off wavelength is calculated as 1288 nm for individual cores. The stress rods are silica doped with 15% molecular fraction of B_2O_3, their RI can be obtained by hybrid Sellmeier equation [25]. Since the beat length less than 5 mm at 1550 nm is helpful to suppress the polarization mixing arising in the SSMF, we further explore the effective RI (Neff), where the stress rods radius r ranges from 6 to 15 μm.

The mechanical parameters are summarized in Table 1, which agree with the practical fiber fabrication condition. Fig. 3(a) depicts the von Mises stress distribution in the transverse cross-section of specialty MCF design [26]. We can see that the stress rods are evenly act on four cores, indicating of that the stress rods provide almost identical birefringence for four cores. Meanwhile, please note that the applied von Mises stress on core 1 and 3 is stretched at x direction but that for core 2 and 4 is at y direction. Consequently, the stress induced birefringence of n_x-n_y in core 1 and 3 are negative while that in core 2 and 4 are positive, as shown in Fig. 3(b), where n_x and n_y are the RI distributions along two orthogonal polarization directions, respectively. As a result, the effective RI of x-polarized eigenstate of polarization (ESOP) is less than that of y-polarized ESOP in core 1 and 3, but larger than that in core 2 and 4, respectively. Thus, we treat x-polarized ESOP in core 2 and 4 as primary ESOP while that in core 1 and 3 as secondary ESOP, where the mode profiles
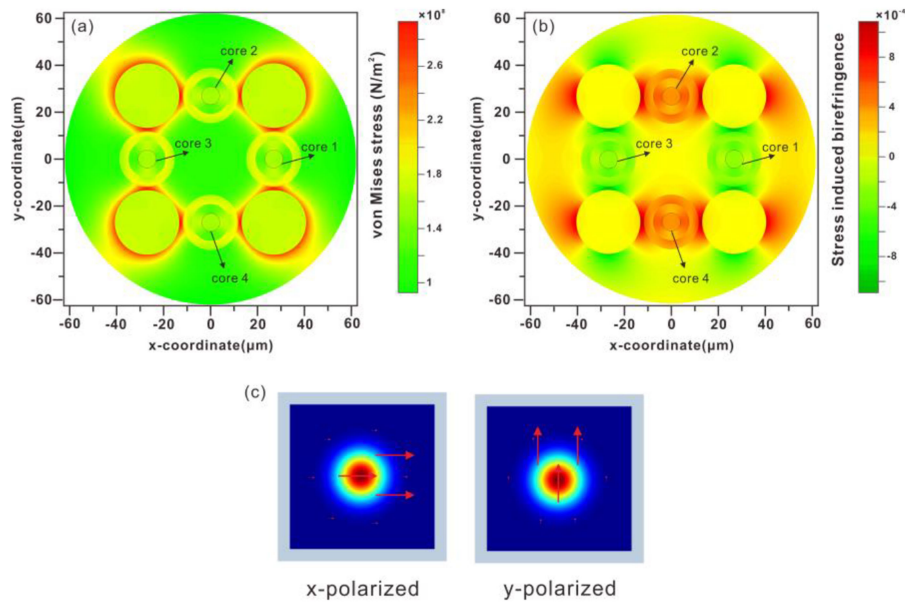
Fig. 3. (a) von Mises stress and (b) stress induced birefringence distribution of the dual panda type 4-core fiber. (c) two ESOPs arising in the individual cores.
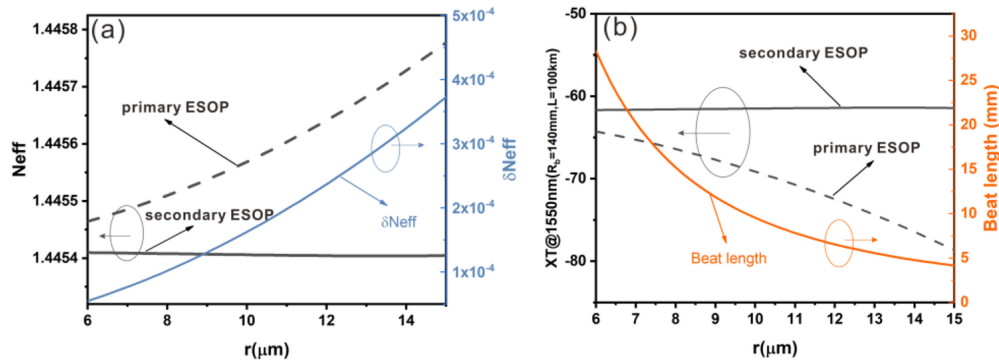

Fig. 4. (a) Effective RIs of two ESOPs, the corresponding δNeff (b) the XT and the beat length of two ESOPs as the function of r at 1550 nm.

of x and y-polarized ESOPs arising in the individual cores are presented in Fig. 3(c). Obviously, the properties of primary and secondary ESOPs arising in the individual cores are identical, due to both homogeneous cores, trench, and stress rods.

Next, when we pay attention to the effective RI of two ESOPs and the corresponding δNeff as the function of r at 1550 nm is shown in Fig. 4(a). The effective RI of primary ESOP is increased with the growing r. However, the effective RI of secondary ESOP is kept almost as constant with respect to the r. Hence, the δNeff between primary and secondary ESOPs is increased by the growing r. δNeff is equals to 1×10^{-4}, when r is equal to 7.93 μm, indicating of the successful mitigation of polarization mixing within the specific core [27]. Since the stress induced birefringence is mainly determined by the radius of the stress rods. Thus, the fabrication accuracy of the stress rod size needs to pay special attention. We find that the birefringence of each core is above 2.78×10^{-4} within the range of r from 13 to 15 μm. Therefore, the designed panda-type 4-core fiber is quite fabrication-tolerant, for the purpose of mitigating the polarization mixing. Meanwhile, due to the orthogonality of two ESOPs, the inter-polarization XT within the specific core is trivial. Furthermore,
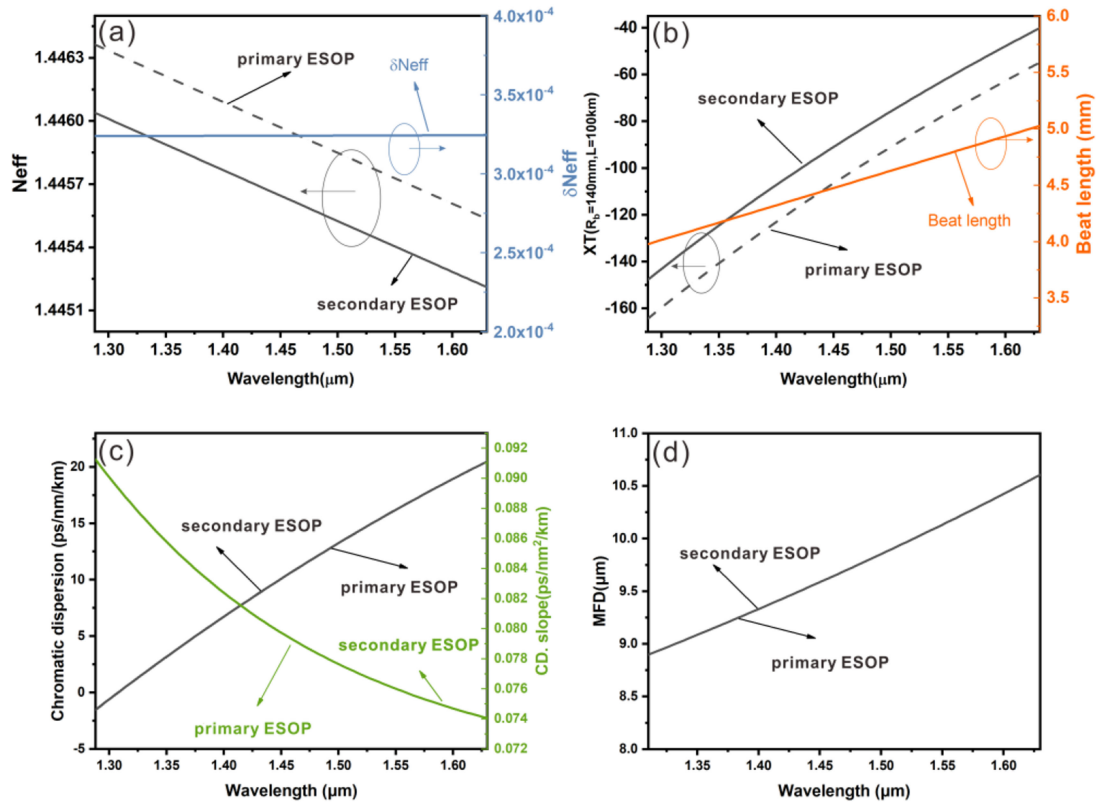
Fig. 5. (a) Effective RIs of two ESOPs, the corresponding δNeff, (b) the XT and the beat length of two ESOPs, (c) the dispersion characteristics, and (d) the MFD from 1288 nm to 1630 nm.

the inter-core XT between adjacent cores for each ESOP and the corresponding beat length are summarized in Fig. 4(b). We can observe that the XT between secondary ESOP changes little, while that of primary ESOP is improved as the increment of r. When r is equal to 15 μm, the inter-core XT for secondary ESOP is −61.4 dB and that of primary ESOP is −78.7 dB, respectively. The results show that the utilization of stress rods not only to improve the birefringence between two ESOPs, but also reinforce the mode field confinement of primary ESOP, because the corresponding effective RI is enhanced by the growing radius of stress rods. Meanwhile, the beat length becomes less than 5 mm when r is larger than 13.7 μm. Moreover, MFD of both two ESOPs arising in each core, which is calculated by the Eq. (3), are nearly equal to 10.15 μm, when r ranges from 6 to 15 μm.

$$MFD = 2 \sqrt{\frac{\left(\iint |E|^2 ds\right)^2}{\pi \iint |E|^4 ds}} \tag{3}$$

At last, when the dual-panda type 4-core fiber is chosen with the following parameters, including $\rho = 4$ μm, r = 14 μm, $\Lambda = 39$ μm, a = 8 μm, w = 4 μm, $\Delta_1 = 0.35\%$ and $\Delta_2 = -0.69\%$, the effective RI and XT of two ESOPs arising in individual cores are numerically calculated from 1288 to 1630 nm. The effective RI, XT, beat length, dispersion characteristics, and MFD for the individual ESOPs are presented in Fig. 5. As shown in Fig. 5(a), although the effective RIs of both two ESOPs are simultaneously reduced with the growing operation wavelength, the δNeff is always more than 3.24×10^{-4}, indicating of the successful mitigation of polarization mixing. Meanwhile, Fig. 5(b) presents the inter-core XT at 1630 nm for primary ESOP is −54.82 dB and that of
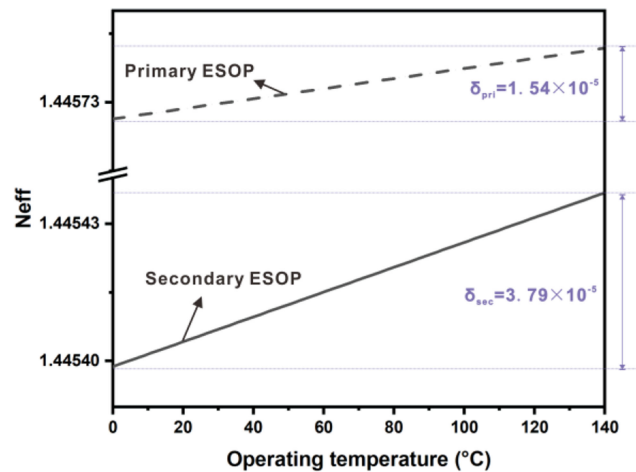
Fig. 6. Effective RIs of two ESOPs as the function of operating temperature.

secondary ESOP is −40.09 dB, respectively. Although the inter-core XT suppression is degraded with the increased operation wavelength, it satisfies the target XT requirement over the O+C+L bands. Furthermore, the input light with arbitrary polarization will be decomposed into primary and secondary ESOPs and then they are independently propagated over the PMF. Consequently, the inter-core XT of proposed four-core fiber generally refers to the power coupling of either primary or secondary ESOP arising different cores. Meanwhile, the beat length increases as the growing operation wavelength. The beat length at 1310 and 1550 nm are 4.05 and 4.78 mm, respectively. Furthermore, we also calculate the chromatic dispersion (CD) and corresponding CD slope for both two ESOPs by using the hybrid Sellmeier equation [28]. Since the effective RIs of both primary and secondary ESOPs vary with the operation wavelength under the same way, their dispersion characteristics are almost the same, as shown in Fig. 5(c), the zero-dispersion wavelength and zero-dispersion slope are 1309 nm and 0.089 ps/nm^2/km for both two ESOPs. The CD values at 1310 and 1550 nm for both two ESOPs are −0.6 and 16 ps/nm/km, respectively. Moreover, the corresponding CD slopes are 0.089 ps/nm^2/km and 0.076 ps/nm^2/km, respectively. Fig. 5(d) show the MFD for both two ESOPs are nearly the same over all wavelength, The MFD of 1310 and 1550 nm for both two ESOPs are 8.9 and 10.1 μm, respectively. As a result, we can draw the conclusion that the specialty four-core fiber can successfully mitigate the polarization mixing under the condition of that the optical properties are comparable to the panda type PM-SMF. At last, the fan-in/fan-out (Fi/Fo) device is necessary to couple the input light from the corresponding SSMF to the individual core of MCF. Recently, we have demonstrated the Fi/Fo devices for 7-core fiber with ultra-low crosstalk of −62 dB [29]. Following the same tapering process, we can easily fabricate the specialty Fi/Fo device for the proposed 4-core fiber.

We further investigate the effective RI variation of two ESOPs, where the operation temperature ranges from 0 to 140 °C. As shown in Fig. 6, the effective RIs of primary and secondary ESOPs are increased with the growing operation temperature. However, the temperature sensitivity of primary ESOP is smaller than that of secondary ESOP, indicating of that secondary ESOP is more susceptible to the operation temperature. Therefore, it is possible to excite two primary ESOPs for the purpose of dual-ring I-FOG implementation. Meanwhile, two secondary ESOPs can be excited for the ease of temperature variation monitoring. Next, we also investigate the bending effect on the four-core fiber by utilizing the conformal mapping method [30]. The birefringence and bending induced loss (α) are calculated as the function of bending radius. The fiber is bent along negative x axis and the bending radius ranges from 10 to 50 cm. As shown in Table 2. We can see that the δNeff for each core are nearly constant over the bending radius range, indicating of that the bending radius has no significant effect on the birefringence for four cores. Moreover, the calculated

TABLE 2
Bending Effect on the Birefringence and Bending Loss

	Bending radius (cm)	10	20	30	40	50	No bend
core 1	δNeff	$3.24{\times}10^{-4}$	$3.24{\times}10^{-4}$	$3.24{\times}10^{-4}$	$3.24{\times}10^{-4}$	$3.24{\times}10^{-4}$	$3.24{\times}10^{-4}$
	maximum α (dB/km)	$8.85{\times}10^{-8}$	$8.82{\times}10^{-8}$	$8.65{\times}10^{-8}$	$8.62{\times}10^{-8}$	$8.62{\times}10^{-8}$	$8.52{\times}10^{-8}$
core 2	δNeff	$3.24{\times}10^{-4}$	$3.24{\times}10^{-4}$	$3.24{\times}10^{-4}$	$3.24{\times}10^{-4}$	$3.24{\times}10^{-4}$	$3.24{\times}10^{-4}$
	maximum α (dB/km)	$8.27{\times}10^{-8}$	$8.26{\times}10^{-8}$	$8.31{\times}10^{-8}$	$8.21{\times}10^{-8}$	$8.23{\times}10^{-8}$	$8.23{\times}10^{-8}$
core 3	δNeff	$3.24{\times}10^{-4}$	$3.24{\times}10^{-4}$	$3.24{\times}10^{-4}$	$3.24{\times}10^{-4}$	$3.24{\times}10^{-4}$	$3.24{\times}10^{-4}$
	maximum α (dB/km)	$8.76{\times}10^{-8}$	$8.43{\times}10^{-8}$	$8.65{\times}10^{-8}$	$8.41{\times}10^{-8}$	$8.33{\times}10^{-8}$	$8.13{\times}10^{-8}$
core 4	δNeff	$3.24{\times}10^{-4}$	$3.24{\times}10^{-4}$	$3.24{\times}10^{-4}$	$3.24{\times}10^{-4}$	$3.24{\times}10^{-4}$	$3.24{\times}10^{-4}$
	maximum α (dB/km)	$8.34{\times}10^{-8}$	$8.29{\times}10^{-8}$	$8.31{\times}10^{-8}$	$8.23{\times}10^{-8}$	$8.23{\times}10^{-8}$	$8.12{\times}10^{-8}$

maximal α, which is the maximal bending induced loss for two ESOPs arising in each core is below 8.85×10^{-8} (dB/km) for all cores among the bending radius range.

3. Conclusions

We report the design strategy of panda type 4-core fiber supporting 8 independent polarization maintaining channels. A large birefringence between two ESOPs arising in individual core is achieved with δNeff of approximate 3.24×10^{-4} from 1288 to 1630 nm. The proposed structure has the advantage of efficient use of stress rods. Our numerical results show that the stress rods can not only enhance the birefringence, but also further suppress the XT at primary ESOP between adjacent cores. Moreover, the result show that the CD characteristic and MFD for two ESOPs arising in the individual core remain the same after the efficient use of the stress rods. In addition, the specialty 4-core-fiber is bending-insensitive among the bending radius from 10 to 50 cm. Such specialty MCF is suitable for both MIMO-free SDM photonic interconnects and compact FOG applications.

References

[1] B Ndagano, I Nape, M. A. Cox, C Rosales-Guzman, and A Forbes, "Creation and detection of vector vortex modes for classical and quantum communication," *J. Lightw. Technol.*, vol. 36, no. 2, pp. 292–301, Jan. 2018.
[2] P. Sillard, D. Molin, M. Bigot-Astruc, A. Amezcua-Correa, K. de Jongh, and F. Achten, "50 μm multimode fibers for mode division multiplexing," *IEEE J. Lightw. Technol.*, vol. 34, no. 8, pp. 1672–1677, Apr. 2016.
[3] L. Wang *et al.*, "Linearly polarized vector modes: enabling MIMO-free mode-division multiplexing," *Opt. Exp.*, vol. 25, no. 10, pp. 11736–11749, 2017.
[4] G. Rademacher *et al.*, "3500-km mode-multiplexed transmission through a three-mode graded-index few-mode fiber link," in *Proc. Eur. Conf. Opt. Commun.*. Gothenburg, Sweden, Sep. 2017, pp. 1–3.
[5] Y. Yang, Q. Mo, S. Fu, B. Liu, M. Tang, and D. Liu, "Panda type elliptical core few-mode fiber," *APL Photon.*, vol. 4, no. 2, 2019, Art. no. 022901.
[6] P. Sillard, M. Bigot-Astruc, D. Boivin, H. Maerten, and L. Provost, "Few-mode fiber for uncoupled mode-division multiplexing transmissions," in *Proc. Eur. Conf. Opt. Commun.*, Geneva, Switzerland, Sep. 2011, pp. 1–3.
[7] R. Ryf *et al.*, "32-bit/s/Hz spectral efficiency WDM transmission over 177-km few-mode fiber," in *Proc. Opt. Fiber Commun. Conf. Exhib.*, Anaheim, CA, USA, Mar. 2013, Paper PDP5A.1.
[8] V. Kamchevska *et al.*, "Experimental demonstration of multidimensional switching nodes for all-optical data center networks," *J. Lightw. Technol.*, vol. 34, no. 8, pp. 1837–1843, Apr. 2016.
[9] G. Milione *et al.*, "1.2-Tb/s MIMO-less transmission over 1 km of four-core elliptical-core few-mode fiber with 125-μm diameter cladding," in *Proc. Optoelectron. Commun. Conf.*, Niigata, Japan, Jul. 2016, Paper PD2-1.
[10] H. Yuan, M. Furdek, A. Muhammad, A. Saljoghei, L. Wosinska, and G. Zervas, "Space-division multiplexing in data center networks: On multi-core fiber solutions and crosstalk-suppressed resource allocation," *J. Opt. Commun. Netw.*, vol. 10, no. 4, pp. 272–288, 2018.
[11] Y. Sasaki *et al.*, "Crosstalk-managed heterogeneous single-mode 32-core fibre," in *Proc. Eur. Conf. Opt. Commun.*, Dusseldorf, Germany, Sep. 2016, pp. 1–3.
[12] R. G. H. van Uden *et al.*, "Ultra-high-density spatial division multiplexing with a few-mode multicore fibre," *Nature Photon.*, vol. 8, no. 11, pp. 865–870, 2014.
[13] T. Hayashi *et al.*, "125-μm-cladding eight-core multi-core fiber realizing ultra-high-density cable suitable for O-band short-reach optical interconnects," *IEEE J. Lightw. Technol.*, vol. 34, no. 1, pp. 85–92, Jan. 2016.

[14] T. Gonda *et al.*, "Design of multicore fiber having upgradability from standard single-mode fibers and its application," *IEEE J. Lightw. Technol.*, vol. 37, no. 2, pp. 396–403, Jan. 2019.

[15] A. Ohno, A. Kurokawa, T. Kumagai, S. Nakamura, and K. Hotate, "Applications and technical progress of fiber optic gyros in Japan," in *Proc. Opt. Fiber Sensors*, MA4, Cancun, Mexico, 2006.

[16] R. Y. Liu, T. F. El Wailly, and R. C. Dankwort, "Test results of Honeywell's first-generation high-performance interferometric fiber optic gyroscope," in *Proc. Fiber Optic Gyros*, Boston, USA, 1992, pp. 262–275.

[17] H. Gu, Y. Cui, and J. Luan, "Angular velocity sensing based on double-ring slow-light structure," *IEEE Photon. Technol. Lett.*, vol. 27, no. 24, pp. 2539–2542, Dec. 2015.

[18] M. J. Grant and M. J. F. Digonnet, "Double-ring resonator optical gyroscopes," *IEEE J. Lightw. Technol.*, vol. 36, no. 13, pp. 2708–2715, Jul. 2018.

[19] G. A. Sanders, R. B. Smith, and G. F. Rouse, "Novel polarization-rotating fiber resonator for rotation sensing applications," *Proc. SPIE*, vol. 1169, pp. 373–381, 1990.

[20] X. Wang, Z. He, and K. Hotate, "Reduction of polarization-fluctuation induced drift in resonator fiber optic gyro by a resonator with twin 90° polarization-axis rotated splices," *Opt. Exp.*, vol. 18, no. 2, pp. 1677–1683, 2010.

[21] H. Ma, X. Yu, and Z. Jin, "Reduction of polarization-fluctuation induced drift in resonator fiber optic gyro by a resonator integrating in-line polarizers," *Opt. Lett.*, vol. 37, no. 16, pp. 3342–3344, 2012.

[22] B. Li *et al.*, "Role of wavelength dependent sensitivity in affecting the crosstalk mitigation of homogeneous multicore fiber: An analytical estimation approach," *Opt. Exp.*, vol. 22, no. 12, pp. 14127–14134, 2014.

[23] K. Okamoto, *Fundamentals of Optical Waveguides*. Elsevier Science, San Diego, CA, 2006, ch. 4.

[24] K. Takenaga *et al.*, "A large effective area multi-core fiber with an optimized cladding thickness," *Opt. Exp.*, vol. 19, no. 26, pp. B543–B550, 2011.

[25] V. Brückner, "To the use of Sellmeier formula," in *Elements of Optical Networking-Basics and Practice of Optical Data Communication*, 1st ed. Berlin, Germany: Springer, 2011, ch. 3.4.1.

[26] R. Guan, F. Zhu, Z. Gan, D. Huang, and S. Liu, "Stress birefringence analysis of polarization maintaining optical fibers," *Opt. Fiber Technol.*, vol. 11, pp. 240–254, 2005.

[27] F. Yaman, N. Bai, B. Zhu, T. Wang, and G. Li, "Long distance transmission in few-mode fibers," *Opt. Exp.*, vol. 18, no. 12, pp. 13250–13257, 2010.

[28] S. Lee, J. Park, Y. Jeong, H. Jung, and K. Oh, "Guided wave analysis of hollow optical fiber for mode-coupling device applications," *IEEE J. Lightw. Technol.*, vol. 27, no. 22, pp. 4919–4926, Nov. 2009.

[29] L. Gan *et al.*, "Ultra-low crosstalk fused taper type fan-in/fan-out devices for multicore fibers," in *Proc. Opt. Fiber Commun. Conf. Exhib.*, San Diego, CA, USA, Mar. 2019, Paper. Th3D.3.

[30] M. Heiblum and J. Harris, "Analysis of curved optical waveguides by conformal transformation," *IEEE J. Quantum Electron.*, vol. 11, no. 2, pp. 75–83, Feb. 1975.